Comparing Manual and Automated Digital Electrode Placement for 12-lead ECG Using MRI-Based Torso Models

Matheus C Faesy[1], Lucas Arantes Berg[2], Daniel K Almeida[1], Filipe L Namorato[1], Daniel M P Leme[1], Camille S dos Santos[3], Zhengda Ma[2], Rafael Sachetto Oliveira[4], Thaiz R Schmal[3], Thiago G S Souza[3], Abhirup Banerjee[2], Blanca Rodriguez[2], Joventino O Campos[1], Rodrigo Weber dos Santos[1]

[1] Universidade Federal de Juiz de Fora, Juiz de Fora, Brazil
[2] University of Oxford, Oxford, United Kingdom
[3] Hospital Universitário de Juiz de Fora, Juiz de Fora, Brazil
[4] Universidade Federal de São João del-Rei, São João del-Rei, Brazil

Abstract

Accurate electrode placement is crucial for reliable ECG simulation. We compare a fully automated method and a semi-automatic approach with expert input for positioning electrodes on MRI-based 3D torso meshes. Both approaches use the same heart model to generate synthetic ECGs via monodomain simulations. While precordial leads showed minor spatial differences, limb electrodes presented large discrepancies, notably LL and RL. Pearson correlation and rRMSE indicated variable waveform similarity across leads. Sensitivity analysis revealed that limb electrodes influence multiple channels, whereas chest electrodes mostly affect their own leads. Results emphasize the importance of anatomically accurate placement in computational ECG workflows.

1. Introduction

Electrocardiography (ECG) remains a widely used diagnostic tool for assessing cardiac function, with its accuracy relying heavily on proper electrode placement on the torso surface [1]. Even small positioning errors can significantly alter ECG waveforms, potentially impacting clinical decisions.

Advances in medical imaging and segmentation have enabled personalized cardiac models from magnetic resonance imaging (MRI) or computed tomography (CT). These 3D reconstructions of the torso and heart capture individual anatomical variability that population-based models may overlook. However, mapping electrodes onto complex 3D surfaces remains challenging due to torso shape variation, conductivity differences, and user expertise [1]. To mitigate this, both automated and semi-automated electrode placement methods have been developed, often integrating image-based tools like 3D Slicer [2].

This study compares two such methods on patient-specific torso meshes: a fully automated pipeline and an expert-guided approach. Using the same heart mesh and stimulus for both, we assess how placement affects ECG morphology, highlighting trade-offs in speed, accuracy, and clinical interpretability.

2. Methods

This study investigates two different approaches for placing electrodes on 3D torso meshes, comparing their performance through ECG simulations using the MONOALG3D software. The meshes were generated after the segmentation of magnetic resonance images from a patient with dilated cardiomyopathy.

Patient Report

This work used data from a 71-year-old male patient who is being monitored at the cardiology outpatient clinic at the University Hospital of the Federal University of Juiz de Fora. He was diagnosed with dilated cardiomyopathy, with a 34% ejection fraction. The patient underwent cardiac MRI (with both cine and late-gadolinium-enhanced sequences). Short-axis images of the heart were used for the segmentations.

Automatic Electrode Placement

The first method consists of an automated pipeline based on [3]. The procedure uses the same MRI dataset to automatically segment both the torso and the heart. The pipeline starts with machine learning-based torso contour extraction, where the scout MR images for each subject are first segmented using a convolutional neural network (U-Net), followed by automated post-processing and refinement through a second network [4]. Extracted contours are then used to fit a statistical shape model (SSM) of the

human body, which is iteratively adjusted to match the extracted contours and form an initial torso mesh. To capture subject-specific anatomical variation, the mesh is further deformed using thin plate splines, with post-processing steps to ensure smoothness and anatomical plausibility. The locations of the ECG electrodes are identified on the mean SSM torso, and their positions are transformed with the mesh such that the resulting torso had electrodes located in equivalent locations. This fully automated workflow minimizes human intervention, ensuring high-speed processing and reproducibility across datasets.

Semi-Automatic and Manual Electrode Placement

The second method integrates semi-automatic segmentation with expert manual annotation. Initially, the torso mesh was segmented from the patient's MRI using TOTALSEGMENTATOR [5], while the cardiac and internal organ structures were extracted using MRSEGMENTATOR [6]. The resulting anatomical meshes were then loaded into a custom-developed interactive application, designed to allow clinicians to manually position the electrodes on the surface of the torso with reference to anatomical landmarks. Figure 1 illustrates interface of this tool.

The application enables physicians to navigate the 3D enviroment, visualize individual anatomical meshes such as the heart, lungs, spine, and torso, and precisely place the 10-lead electrodes by selecting predefined labels. Each electrode can be moved in 3D space using translation arrows, and its position is stored in real time. This environment facilitates accurate placement based on clinical expertise and anatomical landmarks. It is important to note that the rib cage and sternum segmentations were not acquired due to the poor contrast in the MRI scans for these structures. Therefore, placements were instead primarily guided by the torso shape, heart position, and the expertise of the physician.

ECG Simulation and Analysis

For both torso and electrode placements, the heart mesh generated by method in [7] was used to simulate action potential propagation using the monodomain model through the open-source software MONOALG3D [8]. The human-based Ten Tusscher cellular model [9] was employed to describe the cellular dynamics. Cardiac tissue conductivity tensor σ was modeled as anisotropic, incorporating the fiber orientation and a prescribed anisotropy ratio. Temporal discretization was set at $\Delta t = 0.02\ ms$, while spatial discretization was $h = 500\ \mu m$, with $C_m = 1\ \mu F/cm^2$ and $\beta = 1400\ cm^{-1}$. A single electrical stimulus was applied at the apex, and ECG signals were computed at the electrode positions using a pseudo-ECG algorithm.

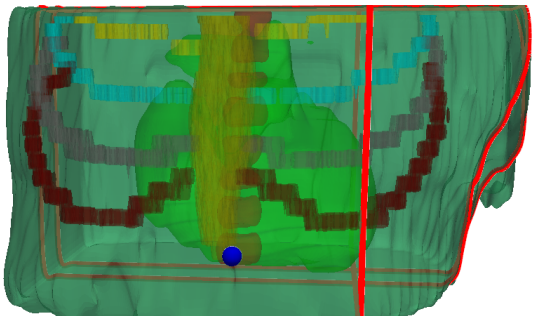

Figure 1: Interface of the custom software used for manual electrode placement.

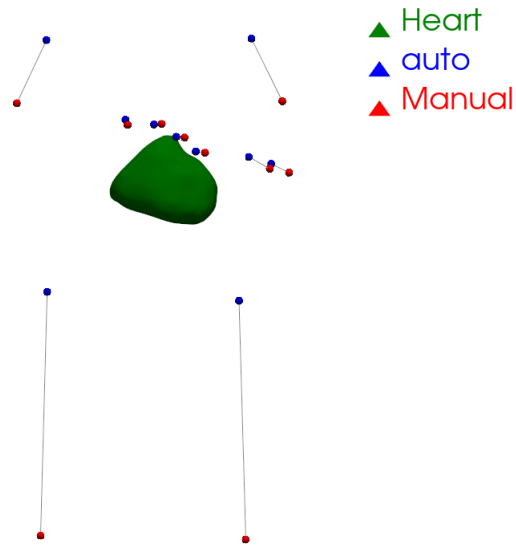

Figure 2: Three-dimensional representation of the torso and heart with manual (blue) and automatic (red) electrode placements. Black lines connect corresponding electrode pairs. Most discrepancies are minimal in the precordial region; larger deviations are observed in limb leads.

3. Results

Figure 2 shows a 3D visualization of the torso mesh along with the manually and automatically placed electrodes. Each pair of corresponding electrodes is connected by a black line to indicate spatial displacement.

To quantitatively evaluate the placement differences between methods, Table 1 presents the spatial displacements between corresponding manual and automatic electrodes. For each lead, we report the differences in X, Y, and Z coordinates (ΔX, ΔY, ΔZ) as well as the Euclidean distance. All values are expressed in millimeters (mm).

Figure 3 shows the ECG waveforms from the 12 standard leads for both manual and automatic electrode con-

Table 1: Spatial difference between manual and automatic electrode positions (in mm).

Lead	ΔX	ΔY	ΔZ	**Distance**
V1	10,250	-6,830	-53,820	55,211
V2	7,740	-7,100	-46,980	48,140
V3	2,330	-6,170	-47,370	47,827
V4	1,080	-1,430	-36,970	37,013
V5	-25,240	-21,810	-41,600	53,323
V6	-24,880	-44,790	-52,130	73,094
LA	33,807	-16,859	-105,777	112,321
LL	965	40,541	-324,419	326,944
RA	-5,787	-14,616	-106,163	107,321
RL	22,229	57,107	-333,049	338,640

figurations. This side-by-side comparison highlights how each lead responds to differences in electrode placement. Blue lines correspond to ECGs generated with manually placed electrodes, while dashed red lines represent the signals using the automatic configuration.

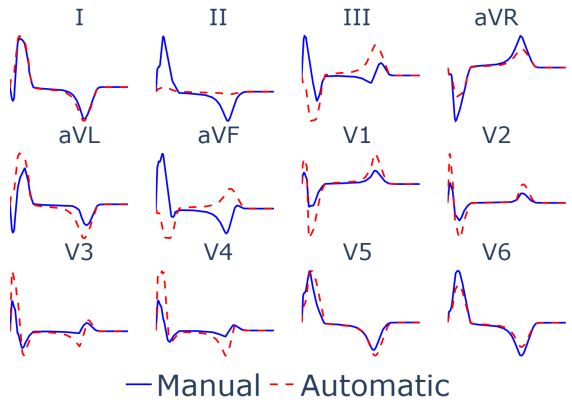

Figure 3: Comparison of 12-lead ECG signals generated from manual (blue) and automatic (dashed red) electrode placements. Each subplot corresponds to a different ECG lead.

Waveform discrepancies can be observed in both shape and amplitude, especially in leads II, III, V2–V6. Some leads show strong agreement in morphology but may differ in amplitude scaling. This visual inspection reinforces the importance of precise electrode positioning, especially for precordial leads sensitive to small spatial shifts.

To quantify the similarity between ECG signals from both placement strategies, we computed the Pearson correlation coefficient (r) and relative root mean square error (rRMSE) for each of the 12 leads. Pearson captures waveform shape and timing, while rRMSE reflects amplitude mismatch. Results showed substantial variability. Among limb and augmented leads, aVF had the highest correlation ($r = 0.98$) but a high rRMSE (≈137%), indicating good shape agreement but amplitude mismatch. Leads II and III also showed strong correlation ($r > 0.96$) with rRMSE over 100%. Precordial leads showed more inconsistency. V1 had moderate agreement ($r = 0.77$, rRMSE = 66.8%), while V6 showed poor similarity ($r = -0.55$, rRMSE = 124.7%), highlighting sensitivity to placement. Leads V2–V5 had rRMSE between 89–117%, despite varying correlations. The overall comparison (all leads concatenated) yielded $r = 0.43$ and global rRMSE ≈101%, showing that the placement method significantly affects ECG morphology. While some leads retain shape similarity, amplitude differences may remain clinically relevant, especially in regions with complex anatomy.

To investigate how sensitive the final multichannel ECG is to variations in individual electrode placement, we conducted a systematic analysis: each automatic electrode was replaced one at a time by its corresponding manual counterpart. After each substitution, a full 12-lead ECG was computed and compared to the original fully automatic configuration. Table 2 summarizes the results of this analysis using the relative root mean square error (rRMSE) for each multichannel lead, expressed as a percentage. Each row in the table corresponds to the substitution of one of the ten electrodes (rows 1 to 10 represent electrodes V1–V6, LA, LL, RA, and RL respectively). Each column shows the resulting rRMSE for a specific lead in the 12-lead ECG system: leads I, II, III, aVR, aVL, aVF, and precordial leads V1–V6.

Table 2: rRMSE (%) for each multichannel lead after replacing one automatic electrode with the manual one.

Lead / Electrode	**I**	**II**	**III**	**aVR**	**aVL**	**aVF**	**V1**	**V2**	**V3**	**V4**	**V5**	**V6**
V1	0	0	0	0	0	0	132	0	0	0	0	0
V2	0	0	0	0	0	0	0	148	0	0	0	0
V3	0	0	0	0	0	0	0	0	93	0	0	0
V4	0	0	0	0	0	0	0	0	0	52	0	0
V5	0	0	0	0	0	0	0	0	0	0	172	0
V6	0	0	0	0	0	0	0	0	0	0	0	202
LA	324	0	28	25	58	14	10	8	6	4	11	23
LL	0	113	118	107	123	115	42	36	25	18	46	98
RA	318	26	0	50	29	13	10	8	6	4	11	23

This analysis serves as a localized sensitivity test, revealing how the final 12-lead ECG is affected when only a single electrode from the automatic configuration is replaced by its manual counterpart. The values in Table 2 represent the rRMSE introduced in each multichannel lead due to such a substitution. As expected, precordial electrodes (V1–V6) exhibit high sensitivity primarily to their corresponding ECG leads, while the rest of the leads remain unaffected. On the other hand, limb electrodes (LA, LL, RA) affect a broader set of leads. These electrodes are involved in the derivation of limb and augmented leads (I,

II, III, aVR, aVL, aVF), and their replacement causes substantial changes in those signals. For instance, replacing the LA electrode (row 7) significantly alters lead I (rRMSE = 324%), aVL (58%), and aVR (25%), and even has moderate effects on precordial leads such as V6 (23%). Interestingly, V6 appeared to be the most sensitive precordial lead to variations in limb electrode positions, particularly those involving LA and LL. This suggests that despite being a chest lead, V6 may be more susceptible to torso-wide field changes introduced by limb placement differences. Among all electrodes, the LL electrode (row 8) resulted in the highest overall sensitivity, impacting nearly all leads with high rRMSE values—most notably II (113%), III (118%), and aVF (115%). This is consistent with the spatial discrepancy observed in Figure 2, where the LL electrode showed one of the largest positional deviations between manual and automatic placement.

4. Conclusion

This study compared a fully automated pipeline and a semi-automatic, expert-driven approach for placing electrodes on MRI-derived 3D torso meshes, aiming to quantify their impact on simulated 12-lead ECG signals. Spatial analyses revealed small discrepancies for most precordial leads (V1–V6), yet limb leads exhibited substantial positional deviations, occasionally exceeding 300 mm. These findings underscore the inherent difficulty in automatically mapping limb electrode positions in a clinical context.

Pearson correlation of the resulting ECG waveforms highlighted that limb-dependent leads can show high concordance (e.g., aVF with $r = 0.9849$) when electrode placement happens to align well, whereas certain precordial leads, such as V6, presented markedly lower correlations ($r = -0.5547$). These differences suggest that even small spatial errors in electrode coordinates can generate significant waveform discrepancies, potentially impacting clinical interpretations.

It is important to highlight that we were unable to determine which method was more accurate due to the absence of segmentations for key anatomical landmarks, such as the rib cage and sternum. In the future, we plan to incorporate CT images, which will enable a more precise evaluation, and expand the number of patients studied. Nevertheless, our results underscore the trade-off between automation and anatomical accuracy, reinforcing the need for more refined strategies in automatic electrode placement.

Acknowledgments

The authors would like to express their thanks to Minas Gerais State Research Support Foundation (FAPEMIG), "Coordenação de Aperfeiçoamento de Emprego de Nível Superior" (CAPES), "Empresa Brasileira de Serviços Hospitalares" (Ebserh), National Council for Scientific and Technological Development (CNPq), SINAPAD Santos-Dumont, and Federal University of Juiz de Fora (UFJF) for funding this work. AB is supported by the Royal Society University Research Fellowship (Grant No. URF\R1\221314).

References

[1] Garcia SL, Torres D, Martinez A, Pueyo E. Impact of electrode positioning on ecg waveforms in personalized cardiac models. Computing in Cardiology 2020;47:1–4.

[2] Pieper S, Fedorov A, Aerts HJ, Frisken S, Kapur T. 3d slicer: A platform for subject-specific image analysis and visualization. Computer Methods and Programs in Biomedicine 2022; 222:106445.

[3] Smith HJ, Rodriguez B, Sang Y, Beetz M, Choudhury R, Grau V, Banerjee A. Anatomical basis of human sex differences in ECG identified by automated torso-cardiac three-dimensional reconstruction. arXiv preprint arXiv231213976 2024;.

[4] Smith HJ, Banerjee A, Choudhury RP, Grau V. Automated torso contour extraction from clinical cardiac MR slices for 3D torso reconstruction. In 44th Annual International Conference of the IEEE Engineering in Medicine & Biology Society (EMBC). 2022; 3809–3813.

[5] Wasserthal J, Meyer M, Zimmerer D, Segeroth M, Full PM, Meine H, Maier-Hein KH. Totalsegmentator: Robust segmentation of 104 anatomical structures in ct images. Medical Image Analysis 2023;84:102680.

[6] Zhou Y, Ma X, Liu C, Huang Y, Li X, Yang G. Mrsegmentator: Automated deep learning tool for whole-body organ segmentation in mri. IEEE Transactions on Medical Imaging 2023;42(5):1234–1245.

[7] Banerjee A, Camps J, Zacur E, Andrews CM, Rudy Y, Choudhury RP, Rodriguez B, Grau V. A completely automated pipeline for 3d reconstruction of human heart from 2d cine magnetic resonance slices. Philosophical Transactions of the Royal Society A Mathematical Physical and Engineering Sciences 2021;379(2199):20200257.

[8] dos Santos RW, Weber GM, Rocha BM, Silva CEB, Rocha BHdP, Weber D, Corrêa AGD. Monoalg3d: A high-performance open-source code for simulating electrical activity in cardiac tissue. Computer Methods and Programs in Biomedicine 2018;164:11–18.

[9] ten Tusscher KH, Panfilov AV. Alternans and spiral breakup in a human ventricular tissue model. American Journal of Physiology Heart and Circulatory Physiology 2006; 291(3):H1088–H1100.

Address for correspondence:

Matheus Cardoso Faesy
Universidade Federal de Juiz de Fora (UFJF) Campus Universitário Rua José Lourenço Kelmer, s/n – Bairro São Pedro CEP 36036-900 – Juiz de Fora – MG, Brasil
matheusfaesy@gmail.com